ADVANCED MATERIALS TECHNOLOGIES
www.advmattechnol.d

Kirigami-Enabled, Passive Resonant Sensors for Wireless Deformation Monitoring

Sadaf Charkhabi, Yee Jher Chan, Doh-Gyu Hwang, Sean T. Frey, Michael D. Bartlett, and Nigel F. Reuel**

A passive resonant sensor with kirigami patterning is presented to wirelessly report material deformation in closed systems. The sensors are fabricated from copper-coated polyimide by etching a conductive Archimedean spiral and then laser cutting kirigami patterns. The sensor response is defined as the resonant frequency in the transmission scattering parameter signal (S_{21}), which is captured via a benchtop vector network analyzer. The sensors are tested over a 0–22 cm range of extension and show a significant shift in resonant frequency (e.g., 90 MHz shift for 10 cm stretch). Furthermore, the effect of resonator coil pitch on the extension sensor gain (MHz cm^{-1}) and linear span of the sensor is studied. The repeatability of the sensor gain is confirmed by performing hysteresis cycles. The sensors is coated with polydimethylsiloxane films to protect from electrical shorting in aqueous environments. The coated resonators are placed in a pipe to report flow rates. The sensor with 1 mm coating is found to have the largest gain (0.17 MHz·s mL^{-1}) and linear span (10–100 mL s^{-1}). Thus, flexible resonant sensors with kirigami-inspired patterns can be tuned via geometric and coating considerations to wirelessly report a large range of extension lengths for potential uses in health monitoring, motion tracking, deformation detection, and soft robotics.

1. Introduction

Position and deformation sensing are critical for applications ranging from virtual reality and robotics to motion tracking and health monitoring.[1–4] These sensors can be used to provide positional feedback for actuator systems,[5,6] estimate the pose and configuration of mechanical or human systems,[7–9] and determine the deformation of a material or structure.[10–12] Recent emphasis on untethered systems requires light, compact, and energy-efficient deformation sensors.[13] Additionally, implementation into wearable sensors for human monitoring and soft robotic systems demand significant extents of deformation.[14–20] Furthermore, wireless monitoring in these systems can reduce system complexity by eliminating or reducing wiring components and can enable more compliant materials by removing semirigid wiring and connection points.[21,22] Thus, wireless monitoring of deformation with passive elements can provide a path forward for deformation sensing in soft bodies for energy-efficient reporting and control.[23]

Wired soft sensors can provide a solution when integrated with wireless communication circuitry (Wi-Fi, Bluetooth, or cellular).[24] These include various designs of stretchable strain sensors, such as dipole, serpentine, spiral, and helical geometries composed of strain-dependent resistive elements such as carbon-impregnated rubbers or compliant microfluidic channels filled with liquid metals.[25–27] In each of these cases, the extra wiring and power consumption of the communication circuitry can limit the utility of untethered applications. Progress is being made on integrating more flexible, wireless sensors for feedback and control of untethered systems. A common solution is imaging, in which motion and position of the device are monitored externally by a camera.[28,29] This works well in structured environments; however, in unstructured environments, where a camera may be blocked or unavailable, this can be a significant challenge. Another approach is the use of resonant sensors to wirelessly report a positional change of soft materials.

Resonant sensors are a long-standing class of passive, wireless sensors that use radio frequency electromagnetic radiation to wirelessly interrogate the scattering parameters of an inductor–capacitor–resistor (LCR) circuit.[30] The resonant circuit responds to changes in the local dielectric (changes circuit capacitance) which has been exploited for measuring physical parameters such as fluid level, pressures, temperature, and biocatalyst activity.[31–39] Flexible LCR sensors have been used to wirelessly measure the strain of compliant materials, such as inductors composed of serpentine copper traces formed as planar[40] or helical coils.[41] In the case of the planar coils, the force is set coplanar to the resonator, and

S. Charkhabi, Y. J. Chan, Prof. N. F. Reuel
Department of Chemical and Biological Engineering
Iowa State University
Ames, IA 50011, USA
E-mail: reuel@iastate.edu
D.-G. Hwang, S. T. Frey, Prof. M. D. Bartlett
Department of Materials Science and Engineering
Soft Materials and Structures Lab
Iowa State University
Ames, IA 50011, USA
E-mail: mbartlet@iastate.edu
The ORCID identification number(s) for the author(s) of this article can be found under https://doi.org/10.1002/admt.201800683.

DOI: 10.1002/admt.201800683

the response is predominantly caused by a change in the self-capacitance[42] (C) of the LCR circuit. In the case of a helical coil, the force is set normal to the spiral plane, the helical distributed length changes, causing a change in inductance (L) which dominates the response. In both cases, the strain causes a geometric change, which causes the resonant frequency of the LCR to shift, however, due to the design of these sensors, they can only report strains of 0–0.3, or in the case of ≈3 cm structures, a deformation of up to 1 cm. Stretchable antennas can also be used to measure deformation; these are primarily based on liquid metals, but recent works have also shown strategies for metallic deformable antennas.[43] However, most examples require connected equipment to transmit data, which limits deployment and deformation tracking in dynamic systems.[44–46] Recently, an elastomer based-liquid metal wireless strain sensor measured deformations up to 50% strain in the radio-frequency range.[47]

Emerging techniques in origami and kirigami engineering offer opportunities to create highly tunable materials and interfaces with complex 3D structures, high extensibility, and tunable stiffness.[48–54] Kirigami is the artistic cousin of origami, in which material is cut (rather than folded) to control structure. In terms of strain or deformation monitoring, most kirigami approaches have used resistive or capacitive measurements, requiring a tethered connection,[55–57] or have used tethered antennas.[58] Wireless kirigami and origami antennas have been demonstrated where the resonant frequency can be tuned based on the extent of folding or deformation.[59–61] However, these demonstrations stop short of exploiting such structures to report the extension length via the resonant scattering parameters of the kirigami antenna. Moreover, these are fabricated to have resonant frequencies suitable for telecommunication (GHz) and not lower frequencies for penetration through water and other biologic media (kHz–MHz range).[62,63]

Herein we present a passive resonant sensor that can be engineered into an extensional sensor with a specific gain and dynamic range based on the pattern of kirigami cuts. The kirigami approach allows this new class of LCR sensors to report much larger deformations normal to their surface (>10× sensor thickness) than previous, encapsulated helical structures.[41] In this work, planar Archimedean copper traces are patterned on a flexible substrate and cut to allow deformation normal to the planar surface, thus exploiting both changes in inductance and self-capacitance. Moreover, we show how the resonator can be coated to protect from an aqueous environment and the effect these coatings have on the sensor gain and dynamic range. Finally, we demonstrate the extensional sensor in a closed system, in this case monitoring the volumetric flow rate of water in a closed pipe (a wireless deflection vane).

2. Results and Discussion

Resonators with fixed outer and inner diameters and varying coil pitch sizes (**Figure 1**a) were fabricated (Figure 1b) from etched copper-coated polyimide (Pyralux) as reported before with the additional steps of coating the resonator with a hydrophobic polymer and laser cutting to release the kirigami coil (see Experimental Section).[39] Pitch (P) is defined as the spacing between the inductive coil lines and the cut is made in the center of the lines (at $P/2$). These resonators were interrogated by stretching vertically in a 24 cm distance between two reader antenna loops (Figure 1c,d; Figure S1, Supporting Information) which were connected to a benchtop vector network analyzer (VNA). For each sensor, the magnitude of the transmission signal (S_{21}) was monitored over a frequency range of 1–300 MHz (Code S2, Supporting Information). By comparing the resonator's S_{21} magnitude from the rest position to an extended state, it was observed that stretching the sensor causes a significant change in the S_{21} response (Figure 1e). This is attributed to a change in the coil's self-capacitance and inductance that is observable in the read range of the interrogating antenna, as described below. The S_{21} response was simplified by tracking the resonant frequency defined as the minimum of the sigmoidal S_{21} feature (160 and 250 MHz in Figure 1e) (Code S3, Supporting Information), as done in other LCR works.[40]

The kirigami resonant sensor response was observed over a wide range of stretch distances (0–22 cm at 1 cm intervals) to determine the linearity of sensor response. A linear increase in the resonant frequency was observed as the sensor was stretched (**Figure 2**) up to a specified length; then the resonant frequency sharply remained constant. The proposed mechanism of this response is a change in both the circuit self-capacitance and inductance. When the kirigami LCR resonator is at rest, the self-capacitance is dictated by the coil to coil spacing.[42] When the resonator is pulled out of plane this spacing is increased, and the capacitance decreases much like the spacing of a parallel plate capacitor (Equation (1)) where C is the capacitance, ε_0 is the permittivity of free space (8.854×10^{-12} F m^{-1}), ε_r is the relative permittivity of the material, A is the capacitive area, and d is the capacitor plate displacement.[64] Additionally, when the resonator with N number of turns is pulled out of plane it resembles a helical coil, where the inductance (L) is defined by (Equation (2)) in which K is the correction factor, l is the axial distributed length, A is the cross-sectional area, and μ_r and μ_0 represent the relative permeability and the permeability of free space, respectively. Thus as the resonator is extended, the length of the coil increases, and the inductance decreases. Since the resonant frequency has an inverse relationship with the capacitance and inductance (Equation (3) where L is the inductance and C is the capacitance),[65] the resonant frequency would increase by extending the resonant sensor. We observe the sharp leveling off of the sensor response (Figure 2b) at the point where all the resonator rings have been lifted off the surface near the interrogating reader antenna. In all geometries tested, the sensor will continue to extend, but the coils begin to warp and the sensor begins to approach a more linear wire geometry, as described below

$$C = \frac{\varepsilon_0 \varepsilon_r A}{d} \tag{1}$$

$$L = K\mu_r\mu_0 \frac{N^2 A}{l} \tag{2}$$

$$\text{Resonant Frequency} = \frac{1}{2\pi\sqrt{LC}} \tag{3}$$

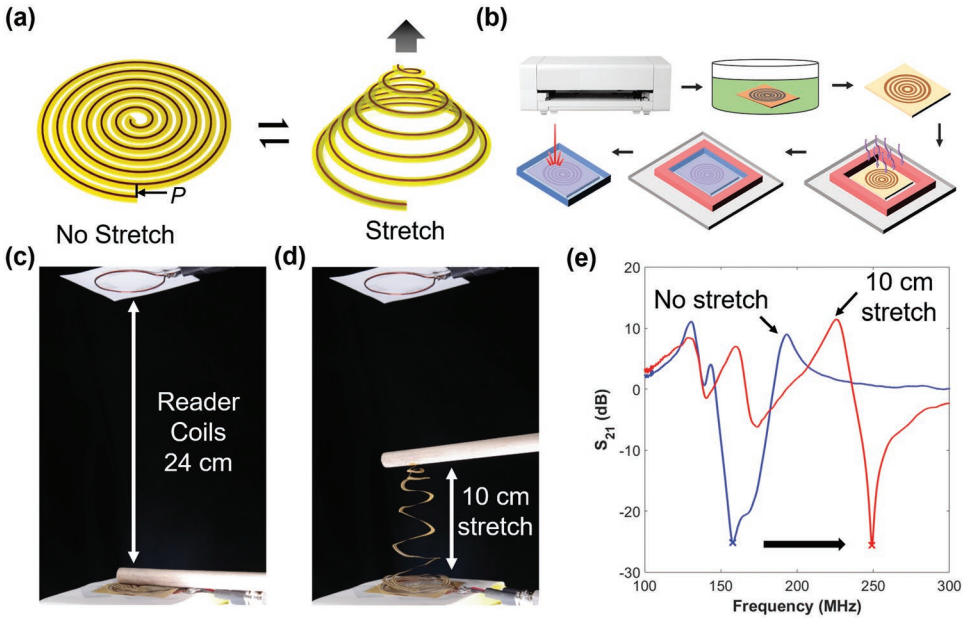

Figure 1. a) Design of a kirigami deformation sensor based on an Archimedean spiral at rest and extended; the pitch (P) is the spacing between the resonant traces. b) The fabrication process of the kirigami resonator which includes patterning the resonator trace, etching, releasing mask, coating, and laser cutting. c) The vertical extension test setup with a 3 mm pitch, 5 mm inner diameter, and 54 mm outer diameter resonator at rest (no extension) and d) with 10 cm extension. e) The S_{21} magnitude response from the sensor in (c,d) depicting the signal minimum used to specify the resonant frequency (marked with "x").

This extension test was repeated for kirigami resonators with different pitches of 3, 4, and 5 mm (Figure 2b). In order to study the effect of the resonator's geometry, we characterize two parameters i) the sensor gain, defined as the linear slope of the frequency versus stretch curve, and ii) the sensor span, defined as the maximum linear deformation the kirigami resonant sensor can report. The gain and span were both found to vary as a function of the resonator pitch. Again, the plateau of the resonant frequency (sensor span) is attributed to the warping and twisting of the kirigami resonant sensor out of the plane of the readers after a certain stretch distance (Video S4, Supporting Information). At this threshold, an increase in extension causes the sensor to twist and elongate, changing from a parallel helical coil to an extended wire perpendicular to the reader loops. This change in deformation pattern, from increasing the coil–coil spacing and helical coil distributed length to a change in perpendicular wire length, would describe this phenomenon. The aforementioned change in capacitance

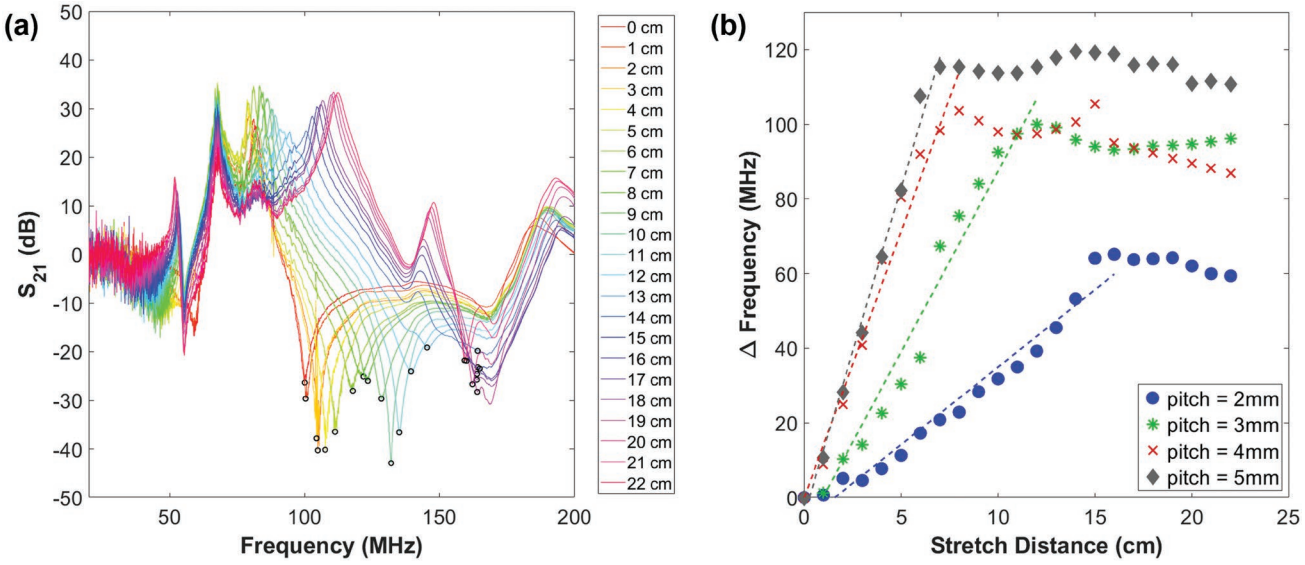

Figure 2. a) Kirigami resonant sensor response found from the minima of resonant frequency peaks (circle points) in the transmission magnitude (S_{21} (dB)) response, scanned over the 0–200 MHz frequency range; data shown here for the 2 mm pitch sensor extended from 0–22 cm. b) Resonant frequency response to different stretch distances for kirigami resonators with varying pitch sizes.

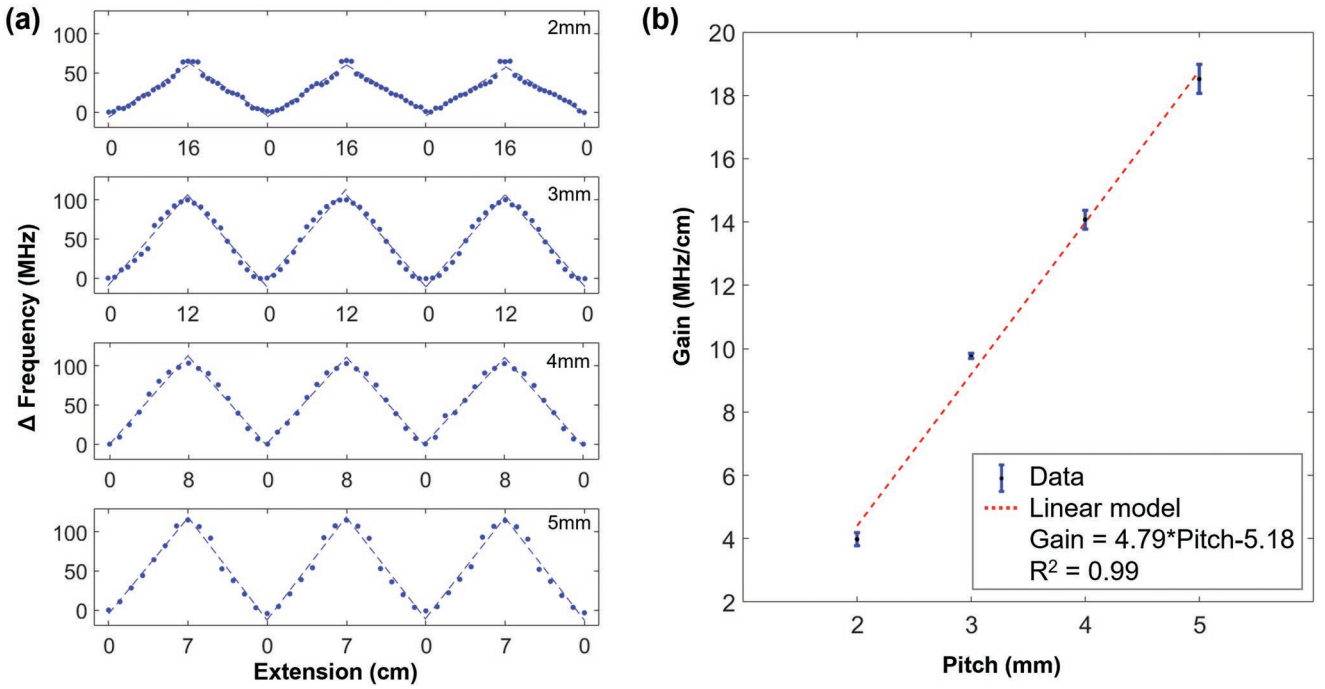

Figure 3. a) Kirigami resonant sensor response in a three-cycle hysteresis experiment to determine the consistency of sensor gain (dashed line fit) for different sensor pitch sizes. b) Gains reported for different pitch sizes and the model (dotted line) showing a linear dependence of gain on pitch size. Error bars refer to one standard deviation for $n = 6$ gains.

and inductance would no longer be dominant during the wire extension phase and the resonant frequency would remain constant. At this point, the circuit begins to approximate a linear antenna, where the resonant frequency is dictated by the length of conductor alone. The sensor span decreases as the pitch size increases. This observation is attributed to the length of the resonator; a smaller pitch corresponds to an inductor-capacitor (LC) sensor with larger length (Table S5, Supporting Information). A longer resonator length allows the coils to stay coplanar for a longer extension length, thus increasing the span of the sensor; however, this also reduces the sensor gain.

To check the reversibility of the sensors, we performed hysteresis experiments in which each sensor was stretched and released three times and the gains were calculated during extension and relaxation (**Figure 3**a). The extent to which the sensor was stretched was modified based on the pitch size to make sure that the response remains in the linear portion of the frequency response (i.e., within the sensor span). Each sensor geometry exhibited a small standard deviation of the gain (Figure 3b). Also, the gain increases linearly with the pitch size of the resonator (equation insert in Figure 3b). As the pitch size increases, the length of the resonator spiral decreases and thus a larger amount of the spiral is pulled out of the interrogation range of the bottom reader coil when extended (Figure S6, Supporting Information), thus causing a more dramatic shift in resonant frequency. The linear model fit to the gain versus pitch data has a high coefficient of determination (R^2) at 0.99, thus demonstrating the ability to choose sensor gain based on kirigami resonator pitch size. Moreover, we cycled the 5 mm pitch resonator to 96 cycles to approximate a sensor that undergoes repetitive extensions (Figure S7, Supporting Information). In this case we found the sensor gain to remain constant, at 14.17 ± 0.20, 14.12 ± 0.10, 14.24 ± 0.14 MHz cm^{-1}, for 1–10, 51–53, and 94–96 cycles respectively (95% confidence intervals).

The next step to embedding these sensors in actual systems is to protect the conductive surface from shorting, especially in water-based applications. Thus, the sensors were coated with polydimethylsiloxane (PDMS) to insulate the LCR resonator from the external environment. For this purpose, the resonator with $P = 5$ mm was chosen as the test candidate since it has the steepest gain (e.g., most responsive). The resonators were coated with varying thicknesses (0.5, 1, and 2 mm cast height, actual height after curing reported in methods) of PDMS by casting the elastomer on the sensor placed within a defined mold. To determine the effect of coating thickness on the sensor gain, three extension hysteresis cycle tests were performed on each resonator in air and the changes in the resonant frequency were measured (**Figure 4**a). The sensor gain was calculated based on each extension and retraction trend (six times in total for each sensor) and was compared for different coating thicknesses (Figure 4b). The maximum extension was kept constant at 7 cm for each sensor.

We first observed that starting resonant frequencies were lower for all coated sensors, which we attribute to the altered dielectric environment. The relative permittivity for air and PDMS is 1 and 2.5 respectively at room temperature which results in a different frequency response window (Figure S8, Supporting Information). Next, we observed a seemingly discontinuous trend in sensor gain as the coating thickness increases (Figure 4b). The uncoated sensor exhibits the highest gain, the minimally-coated sensor (0.5 mm) gain is essentially halved, and then the sensor

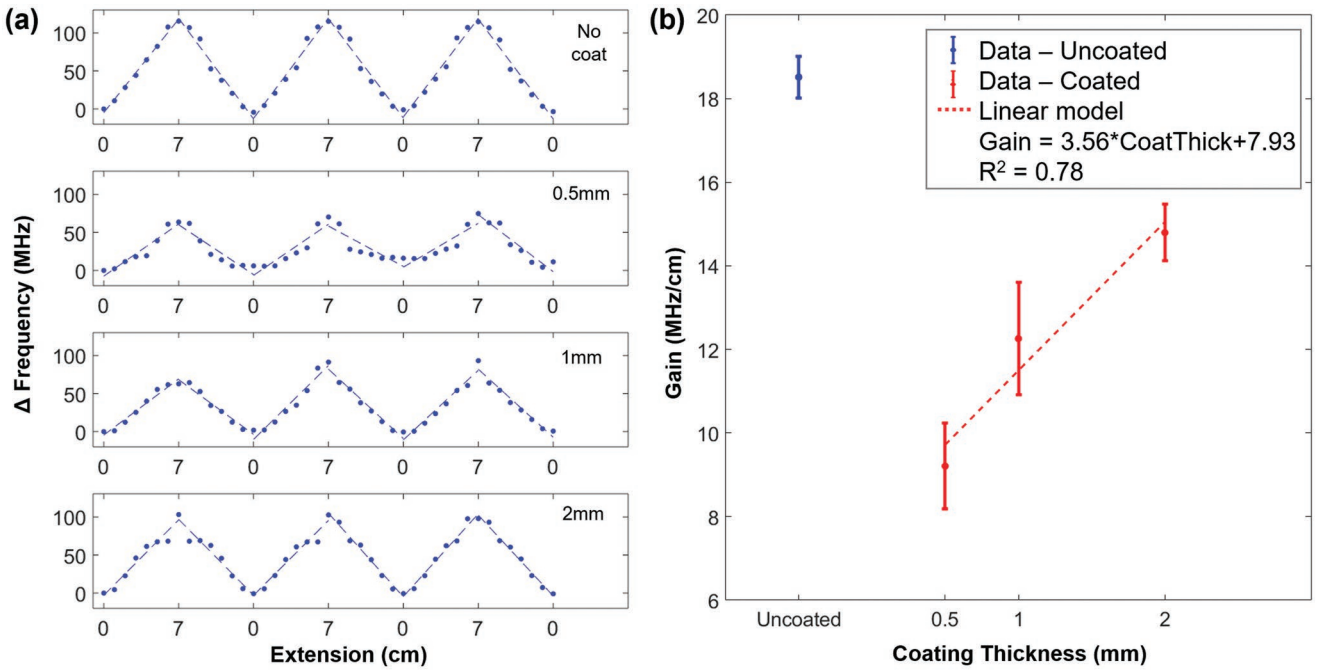

Figure 4. a) PDMS-coated, kirigami resonant sensor response to three hysteresis cycles at 0, 0.5, 1, and 2 mm cast thicknesses of PDMS on a 5 mm pitch sensor showing consistent gains in air (dashed line fit). b) Measured gains for the coated sensors with error bars showing one standard deviation for $n = 6$ gains. Linear model (dashed line) shows a linear relation of gain to coating thickness for 0.5–2 mm coating thickness.

gains increase as the coating thickness is increased. As described above the sensor response is attributed to geometric changes, but in this case, the coil geometry is the same between all sensors; thus the coating must also have an effect on the manner in which the coil unfolds and extends. Upon closer inspection of stretching footage (Figure S9, Supporting Information), we observe that the uncoated coil has very little mass and the polyimide substrate is sufficiently rigid to maintain a regular, helical coil structure. However, the minimal coating adds mass to the coil and due to the large coil compliance, less of the coil length extends from the surface. As the encapsulant coating increases, the coil rigidity increases more rapidly than the added mass and the coil deforms in a manner more similar to the uncoated helical coil. Additionally, we observe an increased variance in the coated resonator gains as compared to the uncoated resonators. This is likely due to the inconsistencies caused by PDMS coating such as stochastic stick–slip phenomena as the PDMS layers rub against each other during extension, which could be reduced in the future, be increasing the cut width.

To determine the applicability of these sensors in a closed system, we utilize PDMS-coated resonant sensors to wirelessly measure the flow rate of liquid in a closed pipe. The sensor was placed in a 6 cm diameter polyvinyl chloride (PVC) pipe (transparent for visual confirmation of extension) oriented vertically (such that gravity pulls down on the sensor) and we measured the effect of flow rate on sensor response (**Figure 5**a). The response was observed using two reader antennas looped externally around the pipe at a displacement of 10 cm and connected to the VNA. The center of the resonator was fixed parallel to the top reader loop while the rest of the coil was free to extend or retract with the water flow. The pipe was initially filled with water and flow rates in the range of 0–100 mL s^{-1} were added via a manual control valve.

As anticipated, increasing the water flow rate increased the resonator's extension length which subsequently increased the resonant frequency. A thicker PDMS coating results in a higher sensor stiffness and decreases the extent to which the kirigami resonator stretches for a given flow rate (Figure 5b; Video S10, Supporting Information). The change in resonant frequency as a function of flow rate was also recorded for different coating thicknesses (Figure 5c). The range of frequency shifts is significantly lower in water when compared to the same resonator in air. We attribute this to the dielectric effect of water ($\varepsilon_r \approx 80$ at 20 °C) which shifts the resonant frequency from 240–370 MHz to 85–100 MHz (Figure S11, Supporting Information). The resonant frequency is dominated by this water effect and thus the effect of extension is less pronounced on these submerged sensors. Also, in the pipe, the kirigami resonator at no flow rate is not flat (as it is in the resting condition measured in air); thus, the effect of extension due to flow rate would again be less than that observed in air.

From the hysteresis plots of the kirigami resonant sensors in a flowing pipe (Figure 5c), we observe that the flow sensor gain (change in frequency response divided by the change in flow rate) was not linear with flow rate (as was observed with uniaxial extension). In **Figure 6**, all the data is presented together, and we clearly observe a threshold flow rate (Q breakthrough, or Q_{BT}) before a linear response is again observed. We attribute the breakthrough flow rate to either the friction between adjacent coils caused by the coating or a nonlinear, force–displacement response of the kirigami. This threshold flow rate increases as the coating thickness increases. A higher variation in the gain

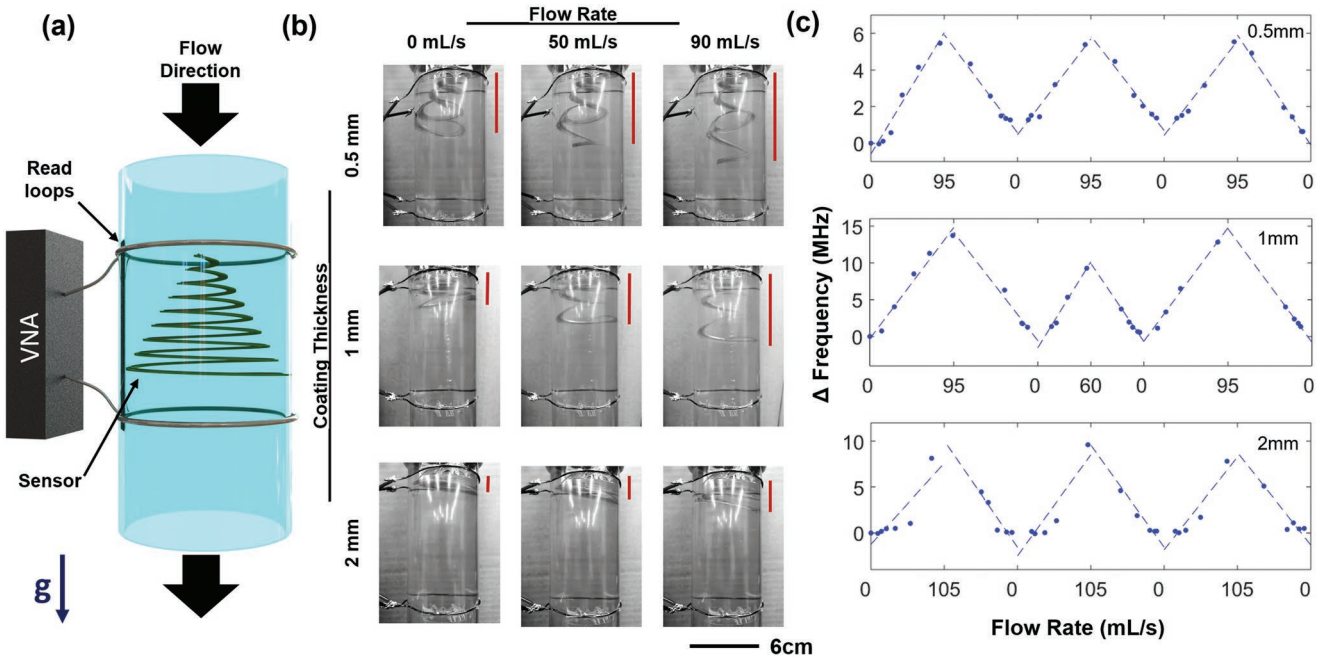

Figure 5. a) Schematic of a kirigami resonant sensor reporting the flow rate of water in a closed pipe. b) Images of the sensor stretching caused by water flow through a clear pipe (Video S8, Supporting Information). c) Three cycle hysteresis experiment to observe changes in the resonant frequency based on the flow rate and dependence on coating thickness. Linear gain model shown with dashed lines.

was observed for thicker coatings, attributed to the stick–slip phenomenon as before. Thicker coatings increase the gain, but if too much is added, it increases the requisite breakthrough flow rate, which would not allow for reporting lower flow rates. From this panel of sensors, the 1 mm coating is optimal since its gain is relatively high and the Q_{BT} is low; however, for a system with low flow rates (below 10 mL s^{-1}), the 0.5 mm coating is suggested since it has no observed breakthrough flow rate. The breakthrough limit is not observed in the preceding air extension experiments as those were conducted at specified extension lengths and do not indicate the force required to reach that extension.

3. Conclusion

Here we demonstrate the design, fabrication, characterization, and application of kirigami resonant sensors for wireless reporting of extension and retraction in closed environments. The sensor response was monitored wirelessly using a vector network analyzer, observing the changes in resonant frequency in the transmission scattering parameter magnitude (S_{21}). Unlike many previously reported resonant deformation sensors, which usually work in millimeter extension ranges, the linearity of this kirigami-inspired resonant sensor can be as high as 16 cm. Furthermore, it was shown that by coating the resonator with PDMS film, the sensor can be applied in both air and aqueous systems. This was demonstrated by wirelessly measuring the flow rate of water in a closed piping system. The kirigami resonator gain exhibits low variability in hysteresis experiments and can be controlled based on pitch size and coating thickness. This portends to their use as reliable and tunable sensors. We anticipate that this type of deformation sensor can be utilized in a variety of applications such as wearable biomonitoring and untethered robotics, where low power,

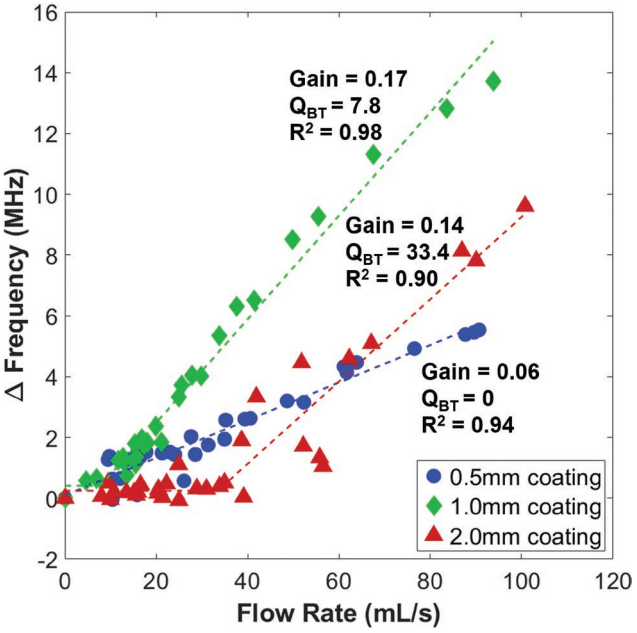

Figure 6. The effect of water flow rate on the changes in resonant frequency for 5 mm pitch resonators with 0.5, 1, and 2 mm cast thickness of PDMS coating affixed in a 6 cm diameter pipe. The data were fit with a linear gain with an additional parameter of a breakthrough flow rate. Reported flow sensor gains, breakthrough flow rate, and model coefficient of determination for each coating thickness are presented on the plot. The units for gain and Q_{BT} are MHz s mL^{-1} and mL s^{-1}, respectively.

wireless sensing combined with high extensibility can enable monitoring and control of future untethered systems.

4. Experimental Section

Fabrication of Resonator for Stretching Test: A circular Archimedean spiral was selected as the pattern for the resonant sensors as it is common, well-characterized in literature,[66] and has a geometry applicable for the intended closed system application (pipe with round cross-section). Archimedean spiral resonant traces having an inner diameter of 2 mm, an outer diameter of 54 mm, and varying pitch sizes in the range of 2–5 mm were designed using Rhino 5 software (Figure 1a). The main reason for choosing the above-mentioned dimensions was to keep the resonant frequency of the coated and embedded kirigami sensors below the microwave frequency to achieve a larger penetration depth in water. The cut trace was patterned as a spiral shape having the same pitch size as the resonator and the inner diameter was modified so that the cut trace would be in the middle of the resonator trace. The resonator trace was patterned on Pyralux sheet, which is a thin copper layer (35 µm) on polyimide (25 µm), using an *X*–*Y* Plotter and an indelible marker (Figure 1b). The Pyralux was then etched in order to remove the unmasked copper using a traditional etchant solution consisting of the 2-1 volumetric ratio of hydrogen peroxide (H_2O_2) and hydrochloric acid (HCl). As the final step for the resonator preparation, the samples were washed with acetone to release the mask. The cut pattern was then created on the resonator sample using a CO_2 laser cutter so that an onion ring-shaped kirigami-based resonant sensor could be fabricated.

Stretching Test Measurement: The kirigami sensor was wirelessly coupled with a reader antenna consisting of two copper loops having a similar diameter of 54 mm and positioned facing toward each other at a 24 cm distance. The reader antenna was connected to a VNA for monitoring the scattering parameters matrix (S-parameters) of the sensor by capturing the phase and the magnitude of the forward transmission (S_{21}) response between 100–500 MHz. A measurement without sensor was first taken to serve as a control, where the subsequent data would be subtracted by that control. The sensor was placed at one end of the copper loop and the center of the sensor was taped to a wooden rod. The sensor was stretched by moving the wooden rod toward the other copper loop. The measurement was taken for every 1 cm movement of the wooden rod until it reached the copper loop at the other end. Then, measurement was taken for every 1 cm of the wooden rod moving backward to its original position. This cyclic experiment was repeated for three times.

Fabrication of Coated Resonators: Spiral resonant traces with no inner diameter and an outer diameter of 42.5 mm were used to fit inside the pipe. The traces were etched using the same approach as described above. After etching, the sensor was placed on an acrylic plate within a mold of set casting thicknesses (0.5, 1.0, and 2.0 mm) and then subjected to oxygen plasma treatment at medium power and 750 mTorr for 5 min to improve bonding application (PDC-001; Harrick Plasma). A batch of PDMS elastomer (Sylgard 184 with a 10:1 oligomer-to-curing agent ratio; Dow Corning) was cast in the mold and cured at 80 °C for 4 h. The heights of the cured films were measured in five places and found to have final heights of 0.47 (±0.1), 0.74 (±0.11), and 1.63 (±0.92) mm (95% confidence intervals). The sealed sample was then laser machined (Epilog Laser Fusion M2, 75 watts) in the spiral pattern.

Resonator Response Measurements under a Flowing System: In this experimental setup, the two copper wire loops were wrapped around a transparent PVC pipe having an inner diameter of 5.08 cm, an outer diameter of 6.03 cm, and a length of 30.5 cm. The distance between the copper loops was 10 cm. With the pipe positioned vertically, the center of the sensor is fixed at the same height as the upper copper loop. A minimal cross-shaped structure made by cellophane tape was connected to the center of the sensor and adhered to the pipe wall. This structure helped to fix the sensor in the middle of the pipe. Fittings were attached to both ends of the pipe and connected to two tubes: 1) a water supply tube at top and 2) drain tube at the bottom. As the direction of water flow in the pipe is parallel to gravity, the system was first filled with water prior to initializing a flow rate to prevent the presence of an air gap within the system. The water flow rate was then tuned by controlling the globe valve of water supply. The water flow rate was determined by measuring the amount of time for the water outlet flow to fill up a 500 mL measuring cylinder. Same VNA device as above was used to read the transmission response (10–500 MHz) for every flow rate tuned. The experiment was started with a small flow rate, slowly increased, then decreased, for three cycles, where 5–7 responses were recorded in each tuning direction.

Supporting Information

Supporting Information is available from the Wiley Online Library or from the author.

Acknowledgements

Funding for this research was provided in part by NSF Industrial Innovation and Partnerships under award 1827578, the Black & Veatch Building a World of Difference Faculty Fellowship to NFR, a 3M Non-tenured Faculty Award to MDB, and Iowa State University startup funds.

Conflict of Interest

The authors declare no conflict of interest.

Keywords

deformation, kirigami, resonant frequency, resonant sensor, wireless sensor

Received: December 5, 2018
Revised: January 28, 2019
Published online:

[1] S. Patel, H. Park, P. Bonato, L. Chan, M. Rodgers, *J. Neuroeng. Rehabil.* **2012**, *9*, 21.
[2] S. Cotin, H. Delingette, N. Ayache, *IEEE Trans. Vis. Comput. Graph.* **1999**, *5*, 62.
[3] S. Kawamura, K. Kanaoka, Y. Nakayama, J. Jeon, D. Fujimoto, in *2003 IEEE Int. Conf. on Robotics and Automation (Cat. No. 03CH37422)*, Vol. *1*, IEEE, Taipei, Taiwan **2003**, pp. 816–821.
[4] C. T. Gentile, M. Wallace, T. D. Avalon, S. Goodman, R. Fuller, T. Hall, *U.S. Patent No. 5,086,785*, Washington, DC, USA **1992**.
[5] P. Gardonio, S. J. Elliott, *J. Sound Vib.* **2005**, *284*, 1.
[6] T. A. Erhart, *U.S. Patent No. 5,557,154*, Washington, DC, USA **1996**.
[7] F. Lorussi, W. Rocchia, E. P. Scilingo, A. Tognetti, D. De Rossi, *IEEE Sens. J.* **2004**, *4*, 807.
[8] F. Lorussi, E. P. Scilingo, M. Tesconi, A. Tognetti, D. De Rossi, *IEEE Trans. Inf. Technol. Biomed.* **2005**, *9*, 372.
[9] P.-C. Lin, H. Komsuoglu, D. E. Koditschek, *IEEE Trans. Rob.* **2005**, *21*, 411.
[10] B. Glišić, N. Simon, *Cem. Concr. Compos.* **2000**, *22*, 115.
[11] C. Cochrane, V. Koncar, M. Lewandowski, C. Dufour, *Sensors* **2007**, *7*, 473.

[12] T. Yamada, Y. Hayamizu, Y. Yamamoto, Y. Yomogida, A. Izadi-Najafabadi, D. N. Futaba, K. Hata, *Nat. Nanotechnol.* **2011**, *6*, 296.
[13] M. Wehner, R. L. Truby, D. J. Fitzgerald, B. Mosadegh, G. M. Whitesides, J. A. Lewis, R. J. Wood, *Nature* **2016**, *536*, 451.
[14] S. Ryu, P. Lee, J. B. Chou, R. Xu, R. Zhao, A. J. Hart, S.-G. Kim, *ACS Nano* **2015**, *9*, 5929.
[15] J. J. Park, W. J. Hyun, S. C. Mun, Y. T. Park, O. O. Park, *ACS Appl. Mater. Interfaces* **2015**, *7*, 6317.
[16] A. M. Nasab, A. Sabzehzar, M. Tatari, C. Majidi, W. Shan, *Soft Rob.* **2017**, *00*, soro. 2016.0039.
[17] M. D. Bartlett, N. Kazem, M. J. Powell-Palm, X. Huang, W. Sun, J. A. Malen, C. Majidi, *Proc. Natl. Acad. Sci. USA* **2017**, *114*, 2143.
[18] R. F. Shepherd, F. Ilievski, W. Choi, S. a Morin, A. A Stokes, A. D. Mazzeo, X. Chen, M. Wang, G. M. Whitesides, *Proc. Natl. Acad. Sci. USA* **2011**, *108*, 20400.
[19] W. Shan, T. Lu, C. Majidi, *Smart Mater. Struct.* **2013**, *22*, 085005.
[20] A. M. V. Mohan, N. H. Kim, Y. Gu, A. J. Bandodkar, J. M. You, R. Kumar, J. F. Kurniawan, S. Xu, J. Wang, *Adv. Mater. Technol.* **2017**, *2*, 1600284.
[21] Y. Jia, K. Sun, F. J. Agosto, M. T. Quiñones, *Meas. Sci. Technol.* **2006**, *17*, 2869.
[22] R. Matsuzaki, A. Todoroki, *Sens. Actuators, A* **2006**, *126*, 277.
[23] J. C. Butler, A. J. Vigliotti, F. W. Verdi, S. M. Walsh, *Sens. Actuators, A* **2002**, *102*, 61.
[24] M. D. Bartlett, E. J. Markvicka, C. Majidi, *Adv. Funct. Mater.* **2016**, *26*, 8496.
[25] J. Zhong, Q. Zhong, Q. Hu, N. Wu, W. Li, B. Wang, B. Hu, J. Zhou, *Adv. Funct. Mater.* **2015**, *25*, 1798.
[26] J. T. Muth, D. M. Vogt, R. L. Truby, Y. Mengüç, D. B. Kolesky, R. J. Wood, J. A. Lewis, *Adv. Mater.* **2014**, *26*, 6307.
[27] J. Lee, S. Kim, J. Lee, D. Yang, B. C. Park, S. Ryu, I. Park, *Nanoscale* **2014**, *6*, 11932.
[28] V. Savage, C. Chang, B. Hartmann, in *Proc. 26th Annual ACM Symp. User Interface Software and Technology*, ACM **2013**, pp. 447–456.
[29] R. Mautz, S. Tilch, in *2011 International Conf. on Indoor Positioning and Indoor Navigation*, IEEE **2011**, pp. 1–7.
[30] H. Bau, N. F. DeRooij, B. Kloeck, *Sensors, Mechanical Sensors*, Vol. *7*, John Wiley & Sons **2008**.
[31] T. J. Harpster, B. Stark, K. Najafi, *Sens. Actuators, A* **2002**, *95*, 100.
[32] K. G. Ong, C. A. Grimes, C. L. Robbins, R. S. Singh, *Sens. Actuators, A* **2001**, *93*, 33.
[33] N. F. Reuel, J. C. McAuliffe, G. A. Becht, M. Mehdizadeh, J. W. Munos, R. Wang, W. J. Delaney, *ACS Sens.* **2016**, *1*, 348.
[34] J. Zhai, T. V. How, B. Hon, *CIRP Ann.* **2010**, *59*, 187.
[35] M. Yvanoff, J. Venkataraman, *IEEE Trans. Antennas Propag.* **2009**, *57*, 885.
[36] C. Li, Q. Tan, W. Zhang, C. Xue, J. Xiong, *IEEE Sens. J.* **2015**, *15*, 1055.
[37] R. A. Potyrailo, W. G. Morris, *Anal. Chem.* **2007**, *79*, 45.
[38] K. G. Ong, J. S. Bitler, C. A. Grimes, L. G. Puckett, L. G. Bachas, *Sensors* **2002**, *2*, 219.
[39] S. Charkhabi, A. Beierle, M. D. McDaniel, N. F. Reuel, *ACS Sens.* **2018**, *3*, 1489.
[40] X. Huang, Y. Liu, H. Cheng, W. Shin, J. A. Fan, Z. Liu, C. Lu, G. Kong, K. Chen, D. Patnaik, *Adv. Funct. Mater.* **2014**, *24*, 3846.
[41] S.-Y. Wu, W. Hsu, *Smart Mater. Struct.* **2013**, *22*, 105015.
[42] A. Massarini, M. K. Kazimierczuk, *IEEE Trans. Power Electron.* **1997**, *12*, 671.
[43] F. Liu, Y. Chen, H. Song, F. Zhang, Z. Fan, Y. Liu, X. Feng, J. A. Rogers, Y. Huang, Y. Zhang, *Small* **2019**, *15*, 1804055.
[44] M. Kubo, X. Li, C. Kim, M. Hashimoto, B. J. Wiley, D. Ham, G. M. Whitesides, *Adv. Mater.* **2010**, *22*, 2749.
[45] J. H. So, J. Thelen, A. Qusba, G. J. Hayes, G. Lazzi, M. D. Dickey, *Adv. Funct. Mater.* **2009**, *19*, 3632.
[46] S. Cheng, A. Rydberg, K. Hjort, Z. Wu, *Appl. Phys. Lett.* **2009**, *94*, 144103.
[47] L. Teng, K. Pan, M. P. Nemitz, R. Song, Z. Hu, A. A. Stokes, *Soft Rob.* **2018**, *00*, 1.
[48] Y. H. Chan, Z. Tse, H. Ren, in *2017 18th Int. Conf. on Advanced Robotics (ICAR)*, IEEE, Hong Kong, China **2017**, pp. 432–437.
[49] D.-G. Hwang, M. D. Bartlett, *Sci. Rep.* **2018**, *8*, 3378.
[50] Z. Yan, M. Han, Y. Yang, K. Nan, H. Luan, Y. Luo, Y. Zhang, Y. Huang, J. A. Rogers, *Extreme Mech. Lett.* **2017**, *11*, 96.
[51] D. G. Hwang, K. Trent, M. D. Bartlett, *ACS Appl. Mater. Interfaces* **2018**, *10*, 6747.
[52] L. Yin, R. Kumar, A. Karajic, L. Xie, J. M. You, D. Joshuia, C. S. Lopez, J. Miller, J. Wang, *Adv. Mater. Technol.* **2018**, *3*, 1.
[53] A. Rafsanjani, Y. Zhang, B. Liu, S. M. Rubinstein, K. Bertoldi, *Sci. Rob.* **2018**, *3*, eaar7555.
[54] M. A. Dias, M. P. McCarron, D. Rayneau-Kirkhope, P. Z. Hanakata, D. K. Campbell, H. S. Park, D. P. Holmes, *Soft Matter* **2017**, *13*, 9087.
[55] A. Firouzeh, J. Paik, *IEEE Sens. J.* **2015**, *15*, 6390.
[56] A. Baldwin, E. Meng, in *2017 IEEE 30th Int. Conf. on Micro Electro Mechanical Systems (MEMS)*, IEEE, Las Vegas, NV, USA **2017**, pp. 227–230.
[57] R. Sun, B. Zhang, L. Yang, W. Zhang, I. Farrow, F. Scarpa, J. Rossiter, *Appl. Phys. Lett.* **2018**, *112*, 1.
[58] Z. Yan, T. Pan, G. Yao, F. Liao, Z. Huang, H. Zhang, M. Gao, Y. Zhang, Y. Lin, *Sci. Rep.* **2017**, *7*, 1.
[59] X. Liu, S. Yao, S. V Georgakopoulos, B. S. Cook, M. M. Tentzeris, in *2014 IEEE MTT-S Int. Microwave Symp. (IMS2014)*, IEEE, Tampa, FL, USA **2014**, pp. 1–4.
[60] S. Yao, X. Liu, S. V. Georgakopoulos, M. M. Tentzeris, *IEEE Antennas Propag. Soc. AP-S Int. Symp.* **2014**, *2*, 374.
[61] H. Fu, K. Nan, W. Bai, W. Huang, K. Bai, L. Lu, C. Zhou, Y. Liu, F. Liu, J. Wang, M. Han, Z. Yan, H. Luan, Y. Zhang, Y. Zhang, J. Zhao, X. Cheng, M. Li, J. W. Lee, Y. Liu, D. Fang, X. Li, Y. Huang, Y. Zhang, J. A. Rogers, *Nat. Mater.* **2018**, *17*, 268.
[62] S. Yao, S. V. Georgakopoulos, B. Cook, M. Tentzeris, in *Microw. Symp. (IMS), 2014 IEEE MTT-S Int.*, IEEE **2014**, pp. 1–4.
[63] X. Liu, S. Yao, B. S. Cook, M. M. Tentzeris, S. V Georgakopoulos, *IEEE Trans. Antennas Propag.* **2015**, *63*, 5897.
[64] W. Bao, A. K. Mondal, J. Xu, C. Wang, D. Su, G. Wang, *J. Power Sources* **2016**, *325*, 286.
[65] L. C. Shen, S. Long, M. Allerding, M. Walton, *IEEE Trans. Antennas Propag.* **1977**, *25*, 595.
[66] S. S. Mohan, M. del Mar Hershenson, S. P. Boyd, T. H. Lee, *IEEE J. Solid-State Circuits* **1999**, *34*, 1419.

ADVANCED MATERIALS TECHNOLOGIES

Supporting Information

for *Adv. Mater. Technol.,* DOI: 10.1002/admt.201800683

Kirigami-Enabled, Passive Resonant Sensors for Wireless Deformation Monitoring

Sadaf Charkhabi, Yee Jher Chan, Doh-Gyu Hwang, Sean T. Frey, Michael D. Bartlett, and Nigel F. Reuel**

Kirigami-enabled, Passive Resonant Sensors for Wireless Deformation Monitoring

Sadaf Charkhabi[1], Yee Jher Chan[1], Doh-Gyu Hwang[2], Sean T. Frey[2], Michael D. Bartlett*[2], and Nigel F. Reuel*[1]

* reuel@iastate.edu for resonant sensors and applications

* mbartlet@iastate.edu for kirigami-enabled soft materials

1. Department of Chemical and Biological Engineering Iowa State University

2. Department of Material Science and Engineering. Soft Materials and Structures Lab. Iowa State University

Contents

1. Figure – Experimental setup

In order to test the effect of the extension on the response profile of the kirigami-enabled resonant sensor, two copper loops having a diameter of 54 mm were placed at 24 cm distance (Fig S1). These reader antennas were connected to a vector network analyzer (VNA) to capture the magnitude of the forward transmission scattering parameter. The sensor was then placed on the bottom reader loop (Loop 1) and stretched vertically toward the top reader antenna (loop 2), as shown by the red arrow in Fig S1, by moving the wooden dowel affixed to the center of the resonator.

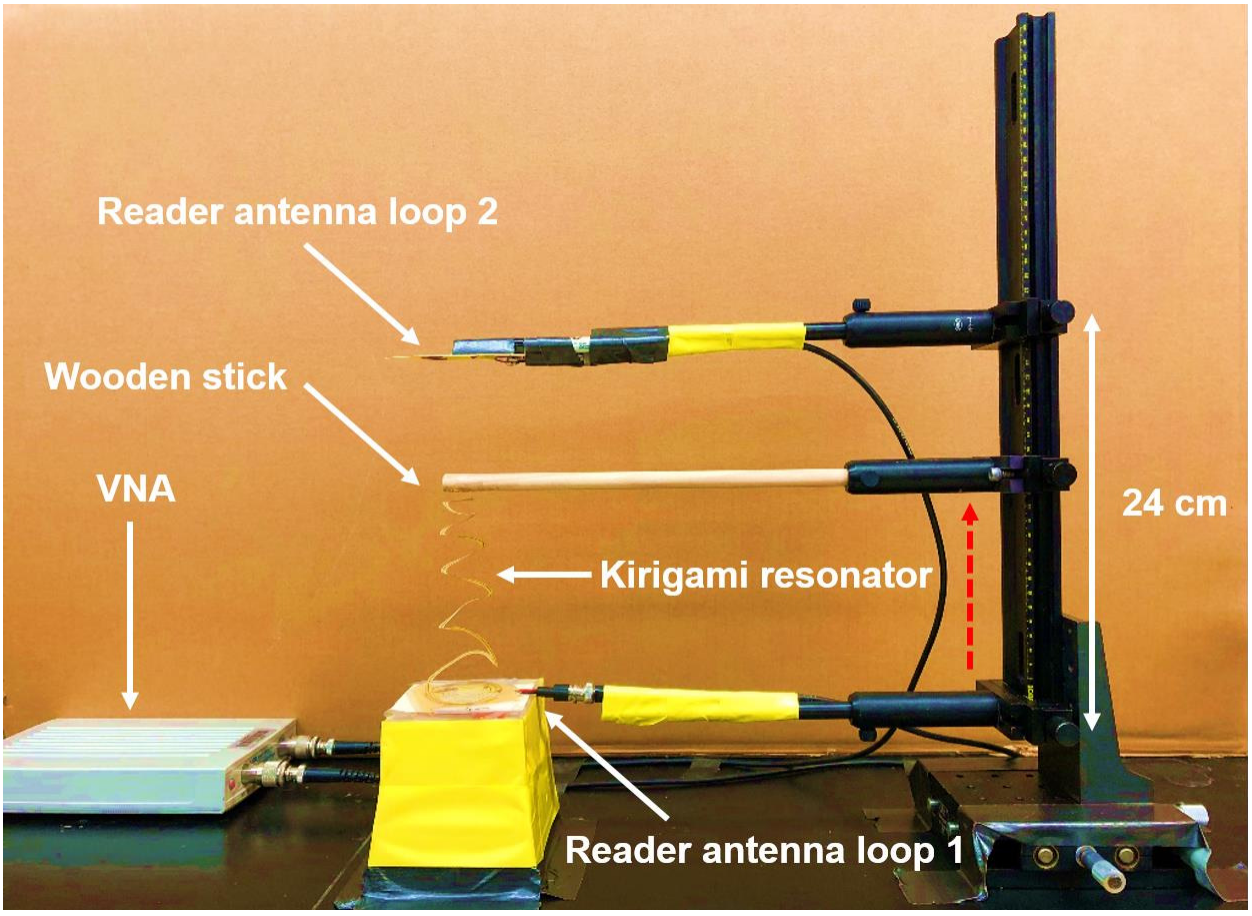

Fig S1 – The experimental setup for the stretching test. The red arrow in the figure represents the direction of the sensor extension.

2. Code – Matlab code for VNA signal capture

In order to measure the kirigami- enabled resonant sensor scattering parameters, we used a two-port VNA (S5048) from Copper Mountain Technologies coupled with the reader antennas as discussed in the experimental setup. The code below was used to take the magnitude of S21 profile over a specific frequency range (dependent on the geometry of the resonator) at 1 cm extension intervals via Matlab (Code S2).

```
function VNADataGrab_v3
% Coded by Nigel F. Reuel on 7.22.2017
% This code interfaces with the copper mountain VNA and takes data at
% specified intervals
% v2 - Updated on May 24, 2018 to record all scattering parameters, also
% updated to use SYSTEM time rather than CPU time to record time between
% measurements...
% Coded for Yee on 5.25.2018
%

% Specify number of measurement points and start/stop freq in MHz
nmp = 5000;
startF = 100;
stopF = 400;
nint = 10; % Number of times the VNA scans and averages (this smooths the
noisy data)
%
% Number of times to run measurement (this is calculated, do not adjust)
%Npts = round(Exptime/Interval);
Npts = input('How many scans are you collecting?');
% Data structure = rows are the different frequencies, C1 = S21
% mlog, C2 = S21 phase, C3 = S11 mlog, C4 = S11 phase (we can ignore the
% other two scattering parameters because they are symmetric with our
% parallel loop reader.
%
for i = 1:Npts
    %t0 = clock;
    Data = zeros(nmp,4);
    [F,Yavg_1] =
vna('S5048',[],startF*10^6,stopF*10^6,nmp,[],'S21','mlog',1,nint);
    [~,Yavg_2] =
vna('S5048',[],startF*10^6,stopF*10^6,nmp,[],'S21','phase',1,nint);
    [~,Yavg_3] =
vna('S5048',[],startF*10^6,stopF*10^6,nmp,[],'S11','mlog',1,nint);
    [~,Yavg_4] =
vna('S5048',[],startF*10^6,stopF*10^6,nmp,[],'S11','phase',1,nint);
    Data(:,1) = Yavg_1';
    Data(:,2) = Yavg_2';
    Data(:,3) = Yavg_3';
    Data(:,4) = Yavg_4';
```

```
    % Insert save function here....what does the data look like from
    if i == 1
        csvwrite('FreqVector.csv',F') % Write the frequency vector on the
first run...
    end
    csvwrite(['Scat_data_',int2str(i),'.csv'],Data)
    % m = 10;
    %t1 = clock;
    %tdif_sec = (etime(clock,t0)) - (etime(clock,t1));
    %pause(Interval-tdif_sec);
    if i < Npts
        pause
    end
end
end

%%%%%%%%%%%%%%%%%%%%%%%%%%%%%%%%%%%%%%%%%%%%%%%%%%%%%%%%%%%%%%%%%%%%%%%%%%%%%%%
%%%
%
%  MATLAB programming example for Copper Mountain VNA
%
%  Version:  1.0
%
%  Author:  Ben Maxson, Copper Mountain Technologies
%           ben.m@coppermountaintech.com
%
%  Support:  support@coppermountaintech.com
%
%%%%%%%%%%%%%%%%%%%%%%%%%%%%%%%%%%%%%%%%%%%%%%%%%%%%%%%%%%%%%%%%%%%%%%%%%%%%%%%
%%%
%
%   Function syntax is as shown below.  [Default] arguments are used if
%   omitted.
%
%   Usage examples:
%   >> vna('S5048')
%
%   >> vna('Planar804',0,10e6,6e9,801)
%
%   >> vna('R54',[],[],[],1601,[],'S11')
%
%
% function output = vna(...
%   instrument,...          %'S5048','S7530','Planar804','Planar304',
%     ...                     %  'S8081' (Planar808/1), 'R54', 'R140',
%     ...                     %  ['TR1300'], 'TR5048', or 'TR7530'
%   use_center_and_span,... %[false] = use fstart/fstop, true = use
center/span
%     f1_hz,...               %[fstart=400e6] or center, as per above, in Hz
%     f2_hz,...               %[fstop=600e6] or span, as per above, in Hz
%     num_points,...          %[401] number of measurement points
%     power_level_dbm,...     %[0] dBm power level (ignored for R54/140)
%     parameter,...           %['S11'], 'S12', 'S22', etc. R54/140 must use
%     ...                     %  'S11'; TR devices must use 'S11' or 'S21';
%     ...                     %  Ports 3 and 4 available for S8081 only
%     format,...              %['mlog'] or 'phase'
%     time_per_iter_sec,...   %[1.0] seconds per measurement interval
```

```
%     num_iter,...            %[10] number of times to loop
%     num_iter_to_store...    %[1] number of function iterations to store
%     )

function [F,Yavg] = vna(...
    instrument,...          %'S5048','S7530','Planar804','Planar304',
    ...                     %  'S8081' (Planar808/1), 'R54', 'R140',
    ...                     %  ['TR1300'], 'TR5048', or 'TR7530'
    use_center_and_span,... %[false] = use fstart/fstop, true = use
center/span
    f1_hz,...               %[fstart=400e6] or center, as per above, in Hz
    f2_hz,...               %[fstop=600e6] or span, as per above, in Hz
    num_points,...          %[401] number of measurement points
    power_level_dbm,...     %[0] dBm power level (ignored for R54/140)
    parameter,...           %['S21'], 'S11', 'S12', etc. R54/140 must use
    ...                     %  'S11'; TR devices must use 'S11' or 'S21';
    ...                     %  Ports 3 and 4 available for S8081 only
    format,...              %['mlog'] or 'phase'
    time_per_iter_sec,...   %[1.0] seconds per measurement interval
    num_iter,...            %[10] number of times to loop
    num_iter_to_store...    %[2] number of function iterations to store
    )

    %%%%%%%%%%%%%%%%%%%%%%%%%%%%%%%%%%%%%%%%%%%%
    %
    %  Assign default parameters to missing
    %   or empty input arguments
    %

    % instrument = 'TR1300'
    if ~exist('instrument','var')
        instrument = 'TR1300';
    elseif isempty(instrument)
        instrument = 'TR1300';
    end

    % use_fcenter_and_fspan = 'false'
    if(~exist('use_fcenter_and_fspan','var'))
        use_fcenter_and_fspan = false;
    elseif isempty(use_fcenter_and_fspan)
        use_fcenter_and_fspan = false;
    end

    % f1_hz = 400e6
    if(~exist('f1_hz','var'))
        f1_hz = 400e6;
    elseif isempty(f1_hz)
        f1_hz = 400e6;
    end

    % f2_hz = 600e6
    if(~exist('f2_hz','var'))
        f2_hz = 600e6;
    elseif isempty(f2_hz)
        f2_hz = 600e6;
    end
```

```
% num_points = 401
if(~exist('num_points','var'))
    num_points = 4000;
elseif isempty(num_points)
    num_points = 4000;
end

% power_level_dbm = 0
if(instrument(1) ~= 'R')
    if(~exist('power_level_dbm','var'))
        power_level_dbm = 0;
    elseif isempty(power_level_dbm)
        power_level_dbm = 0;
    end
end

% parameter = 'S11'
if(~exist('parameter','var'))
    if(instrument(1) ~= 'R')
        parameter = 'S21';
    else
        parameter = 'S11';
    end
elseif isempty(parameter)
    if(instrument(1) ~= 'R')
        parameter = 'S21';
    else
        parameter = 'S11';
    end
end

% format = 'mlog'
if(~exist('format','var'))
    format = 'mlog';
elseif isempty(format)
    format = 'mlog';
end

% time_per_iter_sec = 1.0
if(~exist('time_per_iter_sec','var'))
    time_per_iter_sec = 1.0;
elseif isempty(time_per_iter_sec)
    time_per_iter_sec = 1.0;
end

% num_iter = 10
if(~exist('num_iter','var'))
    num_iter = 10;
elseif isempty(num_iter)
    num_iter = 10;
end

% num_iter_to_store = 2
if(~exist('num_iter_to_store','var'))
```

```
    num_iter_to_store = 1;
elseif isempty(num_iter_to_store)
    num_iter_to_store = 1;
end

%%%%%%%%%%%%%%%%%%%%%%%%%%%%%%%%%%%%%%%%
%
%  Example code
%

%Instantiate COM client
try
    app=actxserver([instrument,'.application']);
catch ME
    disp('Error establishing COM server connection.');
    disp('Check that the VNA application COM server was registered')
    disp('at the time of software installation.');
    disp('This is described in the VNA programming manual.');
    return
end

%Wait up to 20 seconds for instrument to be ready
ready = 0;
count = 0;
while ~ready
    ready = app.ready;
    if count>20,
        disp('Error, instrument not ready.');
        disp('Check that VNA is powered on and connected to PC.');
        disp('The status Ready should appear in the lower right');
        disp('corner of the VNA application window.');

        return
    end;

    %Check every so often whether the instrument is ready yet
    pause(1)
    count = count + 1;
end

%Get and echo the instrument name, serial number, etc.
%
%  [This is a simple example of getting a property in MATLAB.]
%
disp(sprintf(app.name));

%Set the instrument to a Preset state
%
%  [This is an example of executing an ActiveX "method" in MATLAB.]
%
invoke(app.scpi.system,'preset');

%Configure the stimulus
if use_fcenter_and_fspan
    %
```

```
        % [This is an example of getting and setting a property with nested
get
        % statements. Nested gets are needed when an indexed parameter is
        % used (app.scpi.sense[1] in this case).]
        %

set(get(get(get(get(app.scpi,'sense',1),'frequency'),'center'),f1_hz));
        set(get(get(get(get(app.scpi,'sense',1),'frequency'),'span'),f2_hz));
    else
        %
        % [This is an example of getting and setting a property with the
        % subfunction multiget().
        %
        set(multiget(app,'scpi','sense',1,'frequency'),'start',f1_hz);
        set(multiget(app,'scpi','sense',1,'frequency'),'stop',f2_hz);
    end

    set(multiget(app,'scpi','sense',1,'sweep'),'points',num_points);

    if(instrument(1) ~= 'R')

set(multiget(app,'scpi','source',1,'power','port',1,'level','immediate'),'amp
litude',power_level_dbm);
    end

    %Configure the measurement
    set(multiget(app,'scpi','calculate',1,'parameter',1),'define',parameter);
    set(multiget(app,'scpi','calculate',1,'selected'),'format',format);
    set(multiget(app,'scpi','trigger','sequence'),'source','bus');

    tic;
    Yavg = zeros(1,num_points);
    for iter = 1:num_iter

        %Execute the measurement
        invoke(app.scpi.trigger.sequence,'single');

        Y =
get(get(get(get(app.scpi,'calculate',1),'selected'),'data'),'fdata');
        Y = Y(1:2:end);
        Yavg = Yavg + Y;
        F = get(get(get(app.scpi,'sense',1),'frequency'),'data');

        %figure(1);
        %plot(F,Y);
%{
        if iter<num_iter_to_store
            set(app.scpi.mmemory.store,'image',[num2str(iter),'.png']);
            set(app.scpi.mmemory.store,'fdata',[num2str(iter),'.csv'])
        end
%}
        while(toc<iter*time_per_iter_sec)
            pause(0.01);
        end
```

```
    end
Yavg = Yavg./num_iter;
end


function out = multiget(varargin)


    if(nargin==0)           % Nothing to get
        return
    elseif(nargin==1)       % Return the object itself
        out = varargin{1};
    else
        out = varargin{1};  % At least one property is passed in
        idx = 2;
        while idx <= nargin

            %There are at least 2 more arguments not year processed
            if( (nargin - idx) >= 1)

                %If the latter is a number, get the indexed property
                if( isnumeric(varargin{idx+1}))
                    out = get(out,varargin{idx},varargin{idx+1});
                    idx = idx+2;
                    continue;
                end
            end

            %Last argument, or next one's not a number, so there's no index
            %Just get the property itself
            out = get(out,varargin{idx});
            idx = idx+1;

        end

    end

end
```

3. Code – Matlab code for resonant frequency detection

The code below was used for detecting the resonant frequency of the sensor which was defined as the minimum of the S21 magnitude sigmoidal response of the resonator (Code S3). The peaks are selected manually using 'ginput' function. The number of files for each cycle needs to be adjusted if varied.

```
function KirigamiResonatorMinPeakFinding

Stretches1 = [0 1 2 3 4 5 6 7 8 9 10 11 12 13 14 15 16 17 18 19 20 21 22 ...
    21 20 19 18 17 16 15 14 13 12 11 10 9 8 7 6 5 4 3 2 1]';
Stretches2 = [0 1 2 3 4 5 6 7 8 9 10 11 12 13 14 15 16 17 18 19 20 21 22 ...
    21 20 19 18 17 16 15 14 13 12 11 10 9 8 7 6 5 4 3 2 1]';
Stretches3 = [0 1 2 3 4 5 6 7 8 9 10 11 12 13 14 15 16 17 18 19 20 21 22 ...
    21 20 19 18 17 16 15 14 13 12 11 10 9 8 7 6 5 4 3 2 1 0]';

% background data to be subtracted
Backg = csvread(['Scat_data_1.csv']);



% first cycle
for i = 2:45
    F = csvread('FreqVector.csv')./10^6;
    D = csvread(['Scat_data_',int2str(i),'.csv']);
    D = D(:,1);
    DSubtractedBackg = D-Backg(:,1);
    plot(F,DSubtractedBackg)
    grid on
    hold on
    plot(F,Backg(:,1))
    plot(F,D)
    title(Stretches1(i-1))
    hold off
%     xlim([50 150])

    [RF,~] = ginput(1);
    SubtractedF = abs(F-RF);
    [~,approxFreqIndex] = min(SubtractedF);
    while(DSubtractedBackg(approxFreqIndex)>DSubtractedBackg(approxFreqIndex-
1) || DSubtractedBackg(approxFreqIndex)>DSubtractedBackg(approxFreqIndex+1))

if(DSubtractedBackg(approxFreqIndex)>DSubtractedBackg(approxFreqIndex-1))
            approxFreqIndex = approxFreqIndex-1;
        elseif
(DSubtractedBackg(approxFreqIndex)>DSubtractedBackg(approxFreqIndex+1))
            approxFreqIndex = approxFreqIndex+1;
        end
    end
    X = F(approxFreqIndex-20:approxFreqIndex+20,1);
    Y = DSubtractedBackg(approxFreqIndex-20:approxFreqIndex+20,1);
    p = polyfit(X,Y,2);
```

```
    PeakFreq(i-1) = -p(2)/(2*p(1));

    %check data point
    hold on
    peakX = -p(2)/(2*p(1));
    peakY = p(1)*(peakX^2)+p(2)*peakX+p(3);
    plot(peakX,peakY,'o')
    hold off
    title('')
    ylim([-100 40])
    xlabel('frequency (MHz)')
    ylabel('S21')
    legend('Background Subtracted Data','Background','Actual Data','Peak
frequency')

    % save image if needed
%     saveas(gcf,['FirstCycle_',int2str(Stretches1(i-
1)),'_WithBackg_Scat_data_',int2str(i),'.png'])

    plot(F,DSubtractedBackg,peakX,peakY,'o')
    ylim([-50 40])
    xlabel('frequency (MHz)')
    ylabel('S21')

    pause(0.5)

end

% First column = Stretch Distance; Second column = peak frequencies
csvwrite('PeakFreq_HysteresisCycle1.csv',[Stretches1(1) PeakFreq'])



% Second cycle
for i= 46:89
    F = csvread('FreqVector.csv')./10^6;
    D = csvread(['Scat_data_',int2str(i),'.csv']);
    D = D(:,1);
    DSubtractedBackg = D-Backg(:,1);
    plot(F,DSubtractedBackg)
    grid on
    hold on
    plot(F,Backg(:,1))
    plot(F,D)
    title(Stretches2(i-45))
    hold off
%     xlim([50 150])

    [RF,~] = ginput(1);
    SubtractedF = abs(F-RF);
    [~,approxFreqIndex] = min(SubtractedF);
    while(DSubtractedBackg(approxFreqIndex)>DSubtractedBackg(approxFreqIndex-
1) || DSubtractedBackg(approxFreqIndex)>DSubtractedBackg(approxFreqIndex+1))

if(DSubtractedBackg(approxFreqIndex)>DSubtractedBackg(approxFreqIndex-1))
```

```
            approxFreqIndex = approxFreqIndex-1;
        elseif
(DSubtractedBackg(approxFreqIndex)>DSubtractedBackg(approxFreqIndex+1))
            approxFreqIndex = approxFreqIndex+1;
        end
    end
    X = F(approxFreqIndex-20:approxFreqIndex+20,1);
    Y = DSubtractedBackg(approxFreqIndex-20:approxFreqIndex+20,1);
    p = polyfit(X,Y,2);
    PeakFreq(i-45) = -p(2)/(2*p(1));

    %check data point
    hold on
    peakX = -p(2)/(2*p(1));
    peakY = p(1)*(peakX^2)+p(2)*peakX+p(3);
    plot(peakX,peakY,'o')
    hold off
    title('')
    ylim([-100 40])
    xlabel('frequency (MHz)')
    ylabel('S21')
    legend('Background Subtracted Data','Background','Actual Data')

    % save image if needed
%     saveas(gcf,['SecondCycle_',int2str(Stretches2(i-
45)),'_WithBackg_Scat_data_',int2str(i),'.png'])

    plot(F,DSubtractedBackg,peakX,peakY,'o')
    ylim([-50 40])
    xlabel('frequency (MHz)')
    ylabel('S21')

    pause(0.5)

end

% First column = Stretch Distance; Second column = peak frequencies
csvwrite('PeakFreq_HysteresisCycle2.csv',[Stretches2 PeakFreq'])



% Third cycle
for i= 90:134
    F = csvread('FreqVector.csv')./10^6;
    D = csvread(['Scat_data_',int2str(i),'.csv']);
    D = D(:,1);
    DSubtractedBackg = D-Backg(:,1);
    plot(F,DSubtractedBackg)
    grid on
    hold on
    plot(F,Backg(:,1))
    plot(F,D)
    title(Stretches3(i-89))
    hold off
%     xlim([50 150])
```

```
    [RF,~] = ginput(1);
    SubtractedF = abs(F-RF);
    [~,approxFreqIndex] = min(SubtractedF);
    while(DSubtractedBackg(approxFreqIndex)>DSubtractedBackg(approxFreqIndex-
1) || DSubtractedBackg(approxFreqIndex)>DSubtractedBackg(approxFreqIndex+1))

if(DSubtractedBackg(approxFreqIndex)>DSubtractedBackg(approxFreqIndex-1))
            approxFreqIndex = approxFreqIndex-1;
        elseif
(DSubtractedBackg(approxFreqIndex)>DSubtractedBackg(approxFreqIndex+1))
            approxFreqIndex = approxFreqIndex+1;
        end
    end
    X = F(approxFreqIndex-20:approxFreqIndex+20,1);
    Y = DSubtractedBackg(approxFreqIndex-20:approxFreqIndex+20,1);
    p = polyfit(X,Y,2);
    PeakFreq(i-89) = -p(2)/(2*p(1));

    %check data point
    hold on
    peakX = -p(2)/(2*p(1));
    peakY = p(1)*(peakX^2)+p(2)*peakX+p(3);
    plot(peakX,peakY,'o')
    hold off
    title('')
    ylim([-100 40])
    xlabel('frequency (MHz)')
    ylabel('S21')
    legend('Background Subtracted Data','Background','Actual Data')

    % save image if needed
%     saveas(gcf,['ThirdCycle_',int2str(Stretches3(i-
89)),'_WithBackg_Scat_data_',int2str(i),'.png'])

    plot(F,DSubtractedBackg,peakX,peakY,'o')
    ylim([-50 40])
    xlabel('frequency (MHz)')
    ylabel('S21')

    pause(0.5)

end

% First column = Stretch Distance; Second column = peak frequencies
csvwrite('PeakFreq_HysteresisCycle3.csv',[Stretches3 PeakFreq'])



end
```

4. Video – Warping and twisting of Kirigami resonant Sensor

When stretching the kirigami- enabled resonant sensor, the resonator starts to warp and twist after a specific extension point, which is dependent on the geometry of the sensor. This phenomenon can be observed in video S4 (CombinedPitch.avi) for resonators with different pitch sizes.

5. Table – Effect of pitch size on the length of the resonator

The scattering parameter response of the resonant sensor is heavily dependent on the geometrical properties of the resonator. For the Archimedean spiral resonators used in this study, the length of the resonator was controlled by the pitch size since the inner and outer diameters of the spirals were kept constant for different designs (Table S5). As the pitch size increase, the length of the resonator decreases.

Table S5 – Dimension table for resonant sensors.

D_i (mm)	D_o (mm)	P (mm)	L (mm)
2	54	2	1144
2	54	3	763
2	54	4	573
2	54	5	459

6. Figure – Copper loop antenna reading range

The copper loops used as the reader antennas to be coupled wirelessly with the resonant sensor have a reading distance limitation based on their geometry and position. In order to identify the reading range of the 54 mm double loop reader used in this study, a flat resonant sensor was moved upward in the 0-21 cm distance range between the loops at 1 cm intervals. As shown in Fig S6, the signal was strong and detectable with a resonant frequency of about 195 MHz when the resonator was not further than 10 cm from the reader antenna loop 1 (Fig S1). Afterward, the signal starts to weaken as the resonator enters the zone which is not visible by either of the reader loops. As we continue the test, the resonator approaches the reader antenna loop 2 (≥16 cm) and the signal comes back again since the top reader loop starts detecting the resonator.

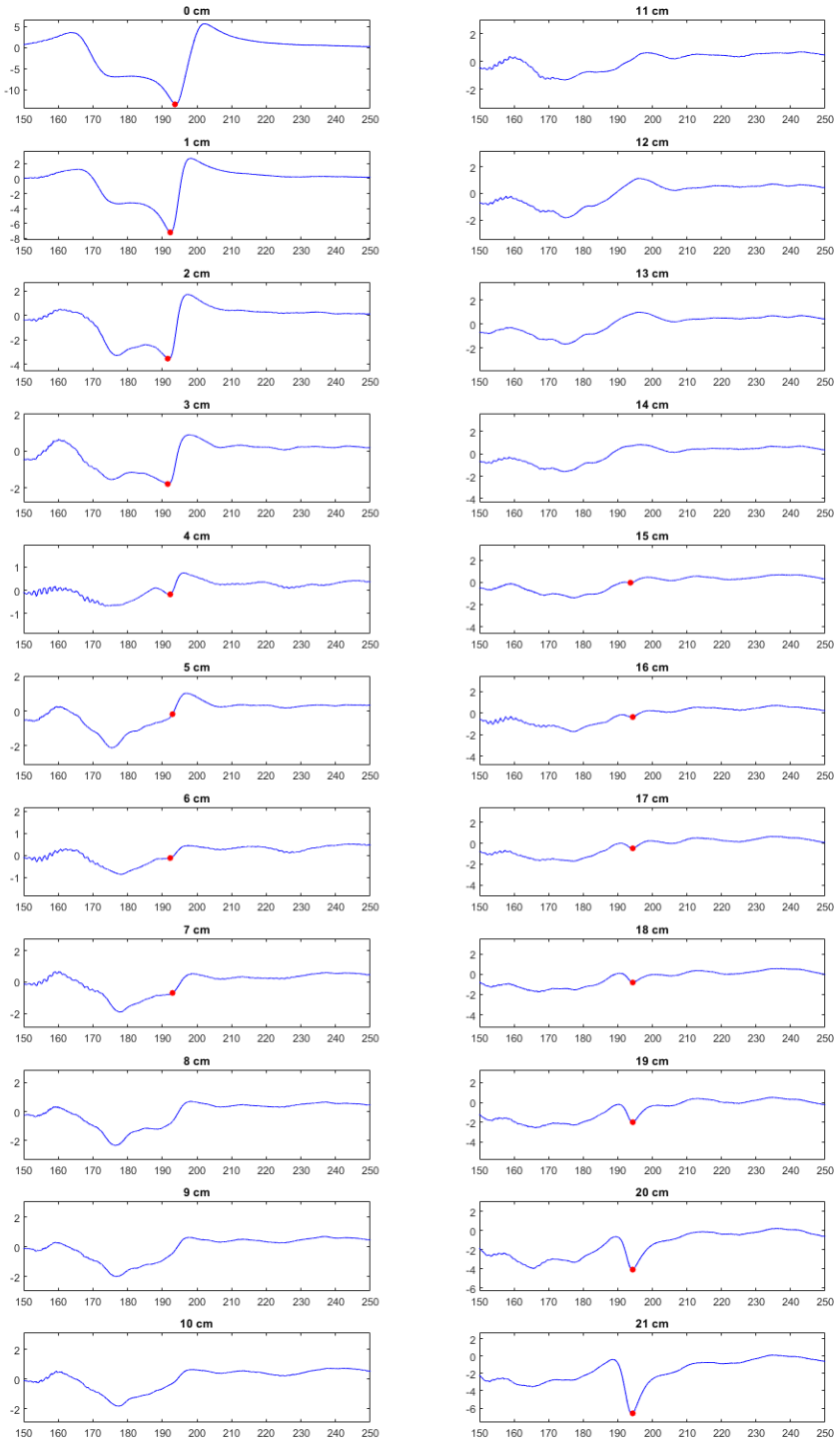

Fig S6 – The S21 profile for a stretch distance range of 0-22 cm; the signal is strong initially for low extensions, weak for the middle range extensions, and strong again for large stretch distances; the peak is around 190-195 MHz.

7. Figure – 96 hysteresis cycle experiment

In order to evaluate the capability of the kirigami sensor to undergo a relatively large amount of stretch and extension cycles, 96 hysteresis cycle test was performed on the uncoated 5 mm pitch resonator in air (Fig S7). The gain values observed for cycles 1-10, 51-53, and 94-96 are 14.17 ± 0.10, 14.12 ± 0.05, and 14.24 ± 0.07, respectively, which indicate a consistent sensor gain for a large level of repetitive extensions.

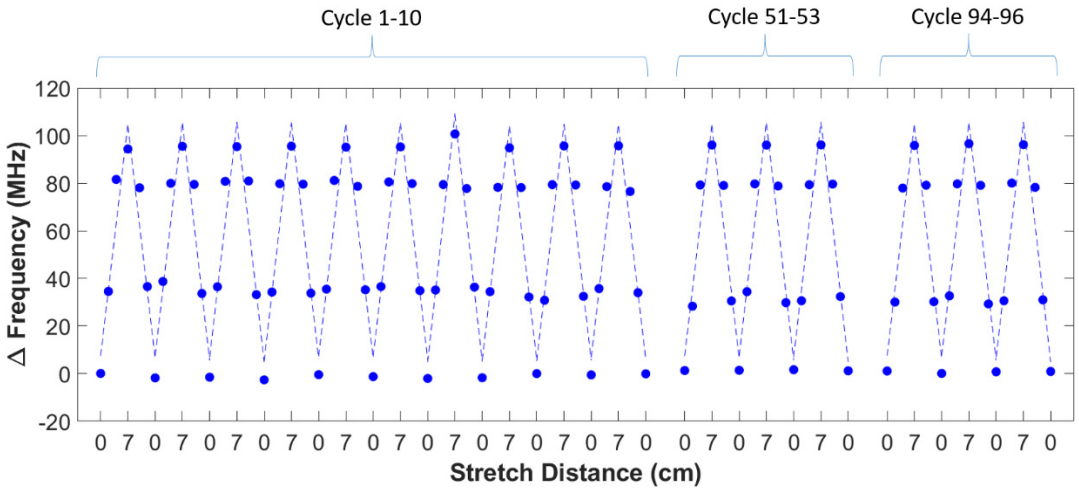

Fig S7 – 96 hysteresis cycle performed on a 5 mm pitch kirigami sensor which was stretched up to 7 cm. The scattering parameter data was captured for displacements of 0, 2, 4, and 7 cm in cycles 1 – 10, 51 – 53, and 94 – 96.

8. Figure – Effect of coating on the resonant frequency

The resonator with 5mm pitch was coated with different thicknesses of PDMS (cast thicknesses of 0.5, 1, and 2 mm) in order to study the effect of coating thickness on the sensor gain. It was observed that the S_{21} response was affected by the PDMS layer due to the differences in the dielectric properties of air and PDMS. As an example, the S21 profile of an uncoated and 2mm coated resonator for 1 and 3 cm extensions are compared (Fig S8).

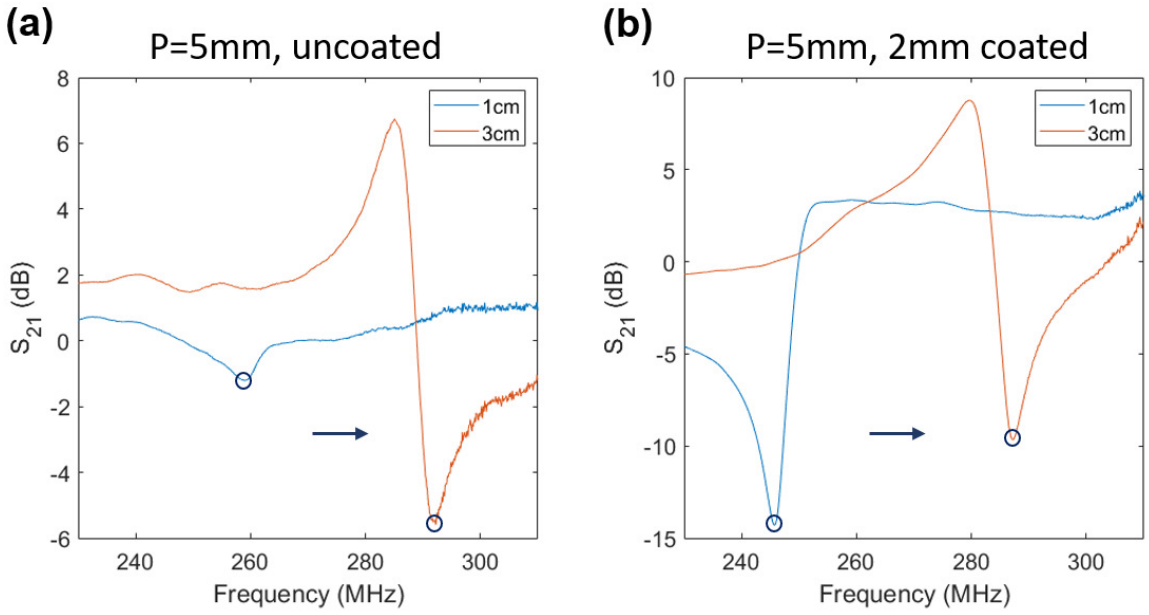

Figure S8 – Effect of coating on the S21 response profile; a) the S21 profile of uncoated 5mm pitch resonator for 1 and 3 cm extension; b) the S21 profile for 2mm PDMS-coated 5mm pitch resonator for 1 and 3 cm extension.

9. Figure – Effect of coating thickness on the sample stretching pattern

The thickness of the coating layer (PDMS) has an effect on the stiffness of the kirigami resonator which results in a different gain value for different coating thickness. The reason is that as the sensor gets stiffer, a larger portion of the length of the resonator is pulled up from the rest state (Fig S9), which is the state in which there is no extension applied on the kirigami resonator. This phenomenon is shown in Fig S8 for 6 cm displacement of the resonators with a similar geometry and different PDMS coating in the range of 0-2 mm.

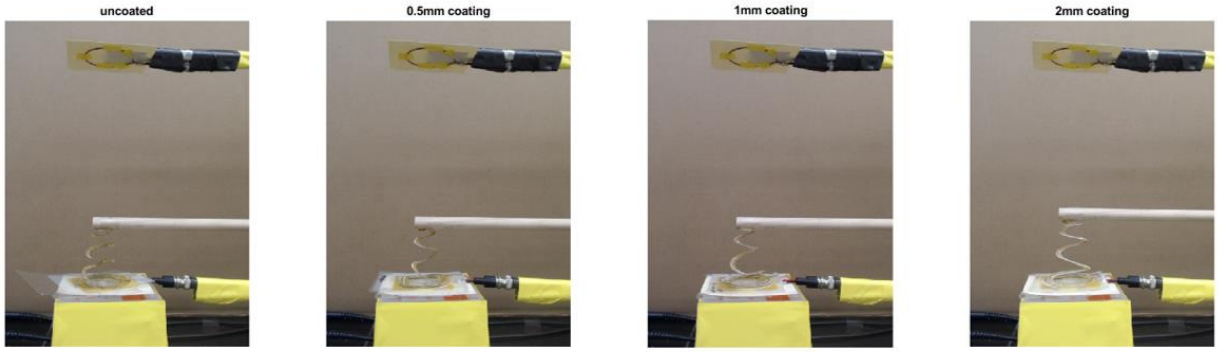

Fig S9 – Effect of coating thickness on the stretching pattern of kirigami resonators for 6 cm displacement.

10. Video – Pipe flow test

The PDMS-coated resonators with different film thicknesses were placed in a transparent PVC pipe in order to study the applicability of the kirigami resonant sensor for measuring the flow rate in a closed system. For all samples, the sensors stretched as the flow rate increased and the extent to which they stretched was dependent on the coating thickness as can be seen in video S10 (CombinedCoating_FlowSystem.avi).

11. Figure – Effect of water on the sensor response

The resonant frequency was significantly lower when the sensor was placed in water pipe compared to the air environment due to the difference in the permittivity values for water and air. Hence, the resonant frequency of the sensor was initially controlled by the presence of water in the system which also affected the changes in the resonant frequency response. Here, we compare the S21 profiles for a sensor with 2mm PDMS coating in air and water for stretch distances of about 1 and 3 cm (Fig S11).

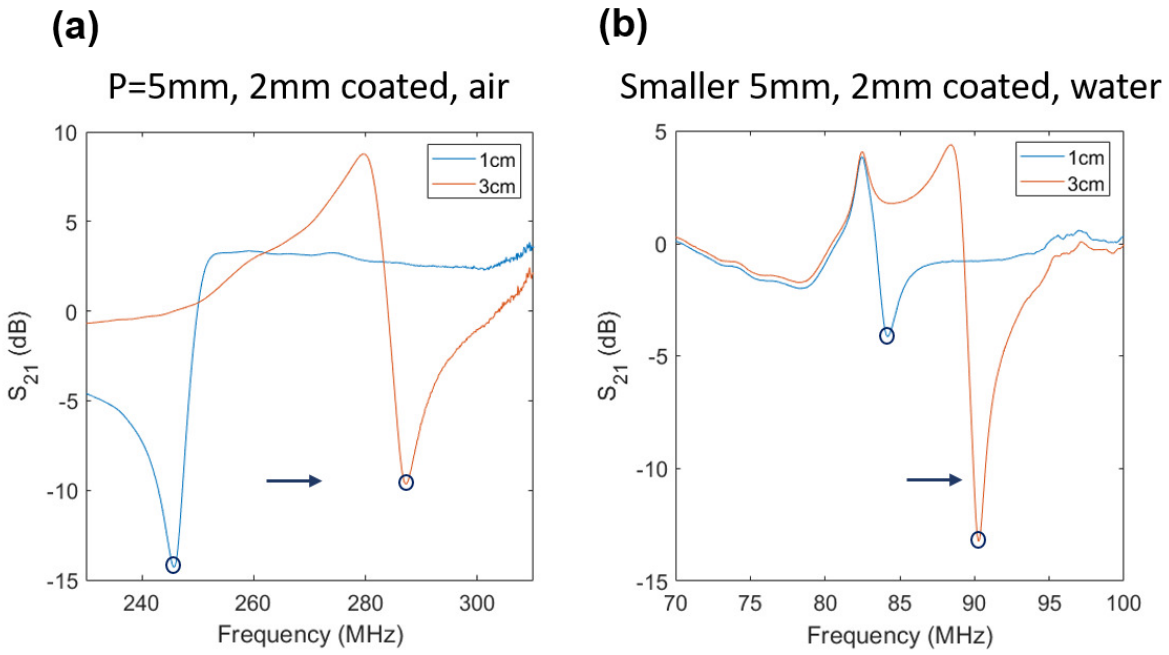

Fig S11 – S21 profile of the resonator with 5mm pitch size and 2mm PDMS coating for 1 and 3cm extensions when a) the resonator is in the air; and b) the resonator is placed in PVC pipe filled with water.